Polar Drive Target Designs for Early NIF Experiments

Ian Gabalski

Webster Thomas High School

Webster, New York

Advisor: Radha P. Bahukutumbi

Laboratory for Laser Energetics

University of Rochester

Rochester, New York

February 2013

1. Abstract

The National Ignition Facility (NIF) is designed to support the indirect-drive irradiation of targets containing fusion fuel. However, direct-drive methods, in which the laser beams directly irradiate the target, are also being explored on the NIF. In order to implode direct-drive targets on the NIF, the indirect-drive configuration must be modified so that the lasers deliver their energy in such a way that the target implodes with a high degree of uniformity. This requires re-pointing the laser beams to adequately illuminate the equator, using laser beam profiles that are not necessarily at best focus, and varying the power in the beams. In order to identify an optimal configuration for these future implosion experiments, different arrangements were explored using the hydrodynamics-modeling code *DRACO*. First, beams were re-pointed towards the equator of the target to maximize initial uniformity. Then, beam powers were adjusted through the remainder of the implosion in order to control the final shape of the target. Control over the final shape was demonstrated in simulations, and a configuration was identified for a uniform direct-drive implosion on the NIF.

Figure 1: (a) Symmetric Direct Drive. Laser beams are arranged symmetrically around the target and hit the surface of the target directly. (b) National Ignition Facility (NIF) Indirect Drive. Lasers are arranged in rings closer to the poles and enter the hohlraum through holes. X-rays emitted by the hohlraum after the laser irradiates its sides drive the target. (c) NIF Direct Drive. Lasers are still arranged in two polar clusters but irradiate the target directly. The poles are over-driven and the equator is under-driven. Several modifications (described in the text) are employed to recover drive uniformity.

2. Introduction

The promise of nuclear fusion is a clean, reliable energy source which does not release large amounts of dangerous or environmentally harmful waste products. However, controlling a fusion reaction in such a way that usable energy is produced in large quantities has proven difficult. The fusion fuel, a mixture of isotopes of elemental hydrogen, must be compressed to thousands of times its solid density while simultaneously being heated. The high temperature is necessary to force the hydrogen nuclei together so that they overcome their electrostatic repulsion and fuse together, forming a helium nucleus and a neutron, and releasing large amounts of energy. The high density is needed to produce enough energy in the form of high-energy neutrons that can be used to produce useful energy.

One proposed method for achieving these conditions is called Inertial Confinement Fusion (ICF). [1] In this method, a small target containing the fuel is irradiated by a high-power laser,

which is designed to deliver its energy simultaneously to a small target of hydrogen fuel enclosed in a shell. The laser heats up the shell, causing the outer portion to ablate outwards while the inner portion is driven inwards. The entire implosion is extremely short in duration, on the order of nanoseconds.

There are two main methods for studying ICF: direct drive and indirect drive. In direct drive, the laser beams are directly incident on the target and deposit their energy. They are usually arranged symmetrically around the target so as to implode it in a uniform manner (Fig. 1a). The OMEGA [2] laser at the University of Rochester is configured symmetrically. In indirect drive, the target is situated in a hohlraum typically made of gold, and the lasers deposit their energy on the inside walls (Fig. 1b). The gold, in turn, emits x-rays, and it is these x-rays which implode the target. The National Ignition Facility (NIF) [3] is primarily configured as in Fig. 1b, except that the shields are not used in current experiments. The main difference between the two laser systems is that while the lasers on OMEGA are arranged in a symmetric fashion around the target, the lasers on the NIF are arranged in a cylindrical configuration, closer to the north and south poles of the target.

While the OMEGA facility is useful in studying the physics of ICF, it does not have enough energy in its laser to achieve ignition; ignition occurs when the helium nuclei begin to deposit their energy back into the fuel, initiating more fusion reactions. Ignition is required to release more energy in the fusion reactions than that which is deposited by the lasers. Simulations indicate that the NIF has adequate energy for ignition, and this is where all of the experiments aimed at achieving ignition are conducted. The NIF is configured to support the indirect drive method. This presents a challenge for direct drive, as the beams are clustered closer to the poles on the NIF (as in Fig. 1c) whereas normally the beams are arranged symmetrically in direct

drive. This would cause the uniformity of a target to degrade rapidly because the poles would implode much faster than the equator. A high degree of uniformity is necessary to conduct a successful ignition experiment because otherwise the fuel will not be compressed to the densities and temperatures necessary for fusion reactions.

The solution to this problem is a method known as polar drive. This entails modifying the configuration of the laser system in such a way that the target implodes uniformly. Generally, this involves a variety of changes. Each beam on the NIF has a phase plate, which defines a spatial shape and diameter at best focus. Existing NIF phase plates are designed for indirect-drive ignition with the constraint that the beams must fit through the laser entrance hole. These beam spot sizes are small and elliptical in shape, and can introduce long wavelength nonuniformities from the asymmetry in the laser drive. Following Ref. 4, beams are defocused to reduce the level of nonuniformity introduced into the beam shapes. In addition, beams are repointed towards the equator to compensate for the lack of irradiation there. Finally, beam powers are adjusted throughout the implosion to provide additional control of the shape of the shell. Since symmetry is a significant challenge for polar drive, preliminary NIF experiments are required to explore the feasibility of a successful polar drive ignition experiment.

In the present work, the 2D hydrodynamics modeling code *DRACO* [5] was used to simulate implosions and identify an optimal configuration which may be used in future experiments. A systematic approach was employed which first modified only beam pointing in order to maximize the initial uniformity of the implosion. After this was accomplished, beam energy changes were used to establish control over the shape of the shell as it is imploded and to identify a configuration which yields a uniform implosion.

3. Beam Pointing Modifications

The NIF has 192 beams, which are grouped into 2x2 arrays, called quads. In this work, each quad is treated as a unit, and all the beams in a quad have the same beam profiles, are defocused to the same extent, and have the same laser-pulse temporal history. Furthermore, the quads are arranged into 4 rings, and all quads in a ring are pointed at the same polar angle while varying in azimuthal angle. There are 24 quads clustered at the north pole of the target and 24 at the south. Figure 2a shows the positions of the northern quads on target with the original NIF configuration. There is reduced irradiation from 50° to 90°, relative to the pole. Fig. 2b gives the normalized initial intensity as a function of polar angle, illustrating that little energy is deposited near the equator. In order to compensate for this issue, a re-pointing scheme was developed and simulated in *DRACO* (Fig. 2c). The initial on-target intensity of the optimized configuration is given in Fig. 2d. The higher intensity at the equator is required to compensate for the reduced energy absorption from the oblique angles of incidence of the repointed beams.
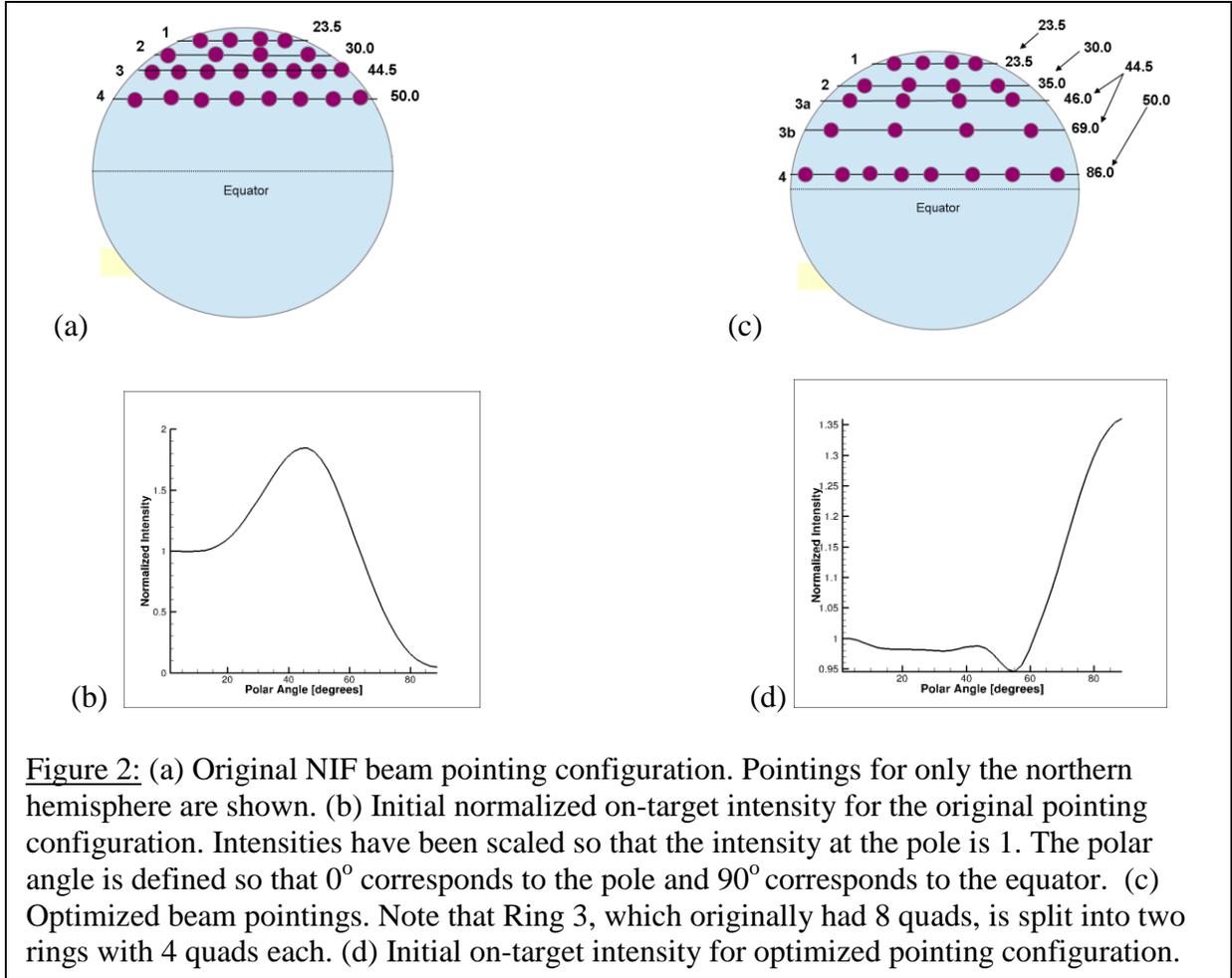
Figure 2: (a) Original NIF beam pointing configuration. Pointings for only the northern hemisphere are shown. (b) Initial normalized on-target intensity for the original pointing configuration. Intensities have been scaled so that the intensity at the pole is 1. The polar angle is defined so that 0° corresponds to the pole and 90° corresponds to the equator. (c) Optimized beam pointings. Note that Ring 3, which originally had 8 quads, is split into two rings with 4 quads each. (d) Initial on-target intensity for optimized pointing configuration.

An 1100-µm-radius room temperature target with an 80-µm-thick plastic CH shell was simulated (Fig. 3a). The target is driven by a laser pulse that has a low-intensity foot (defined as the initial constant power until approximately 2 ns) and a slow rise to a constant-power main pulse. The purpose of the foot is to launch a shock and to begin driving the target inward. However, the target must be compressed adiabatically, meaning that it is not heated in the process, because a preheated target is difficult to compress to densities necessary for fusion. In order to achieve this, the foot has a low power relative to the remainder of the pulse. The duration of the foot is tailored so that it ends at shock breakout, which is approximately 1.5 ns for these designs. After the foot ends, the power increases during the "rise" portion of the laser pulse
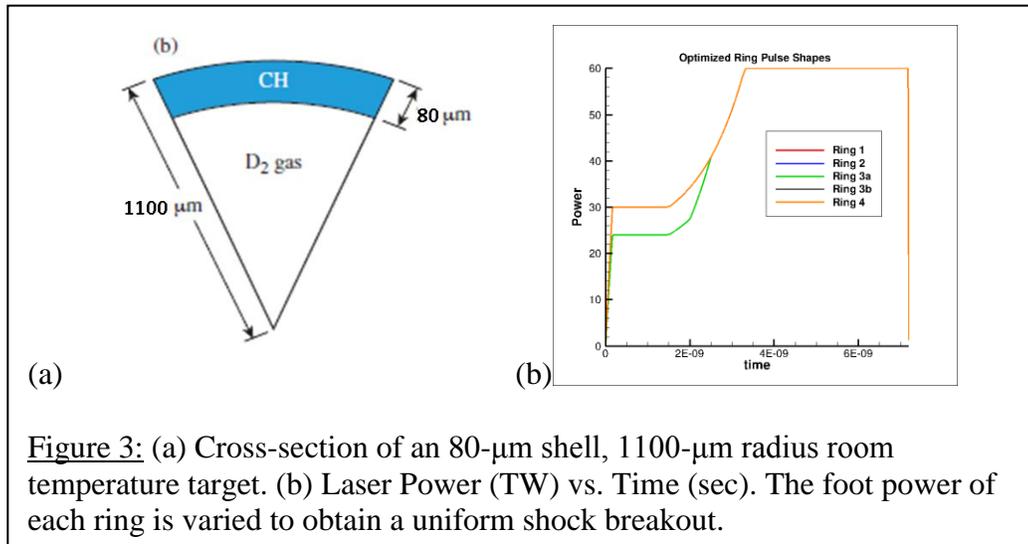
Figure 3: (a) Cross-section of an 80-μm shell, 1100-μm radius room temperature target. (b) Laser Power (TW) vs. Time (sec). The foot power of each ring is varied to obtain a uniform shock breakout.

up to its maximum value. The rise of the pulse is designed to adiabatically compress the target. Finally, the main pulse delivers most of the energy necessary to compress the shell and provides its kinetic energy.

It is necessary to keep the initial conditions of the implosion as uniform as possible because any nonuniformity which is introduced early on in the implosion will grow due to the converging shell. When the laser initially begins to irradiate the target, it launches a shock wave which compresses the target and moves inward faster than the shell. It is the uniformity of this shock which determines the overall initial uniformity of the target. The shock moves through the shell first, compressing it, and then breaks out of the shell and moves into the internal gas. This point in the implosion where the shock changes between media is called "shock breakout," and this was the point when the uniformity of the shock was determined in the simulation. The pointings of the quads were varied to minimize this nonuniformity.

Three changes to the laser were employed to achieve uniformity. First, the foot of the laser pulse was modified by an overall multiplier (Fig. 3b). These multipliers were iteratively selected; Rings 1, 3b, and 4 use a multiplier of 1.0, whereas Rings 2 and 3a reduce the energy in

the foot by using a multiplier of 0.8. Second, the beams were defocused using the technique described in Ref. [4]. Third, beams were re-pointed away from the center of the target so as to adequately irradiate the equator (Fig. 2c). In conjunction with this, Ring 3 was split into two separate rings so that there was more flexibility with the pointings of its eight quads. Once a semi-uniform configuration was identified, the polar angle of each ring was systematically changed by $\pm 3^{\circ}$ to identify the most uniform case. The optimized configuration is the same as the one shown in Figure 2c.

In Figure 4, a density contour plot of the northern hemisphere of the target is given at shock breakout, shown in radius vs. polar angle to demonstrate how much the shock deviates from uniform from pole to equator. Fig. 4a shows a nonuniform shock breakout obtained simply by an arbitrary repointing of the beams and Fig. 4b shows a more uniform shock breakout, corresponding to the pointing configuration shown in Figure 2c. The optimized configuration was identified simply by examining these plots of shock breakout for a variety of different pointing changes and deciding on the most uniform case. It can be seen that varying the pointing of the beams has a direct impact on the uniformity of the shock.
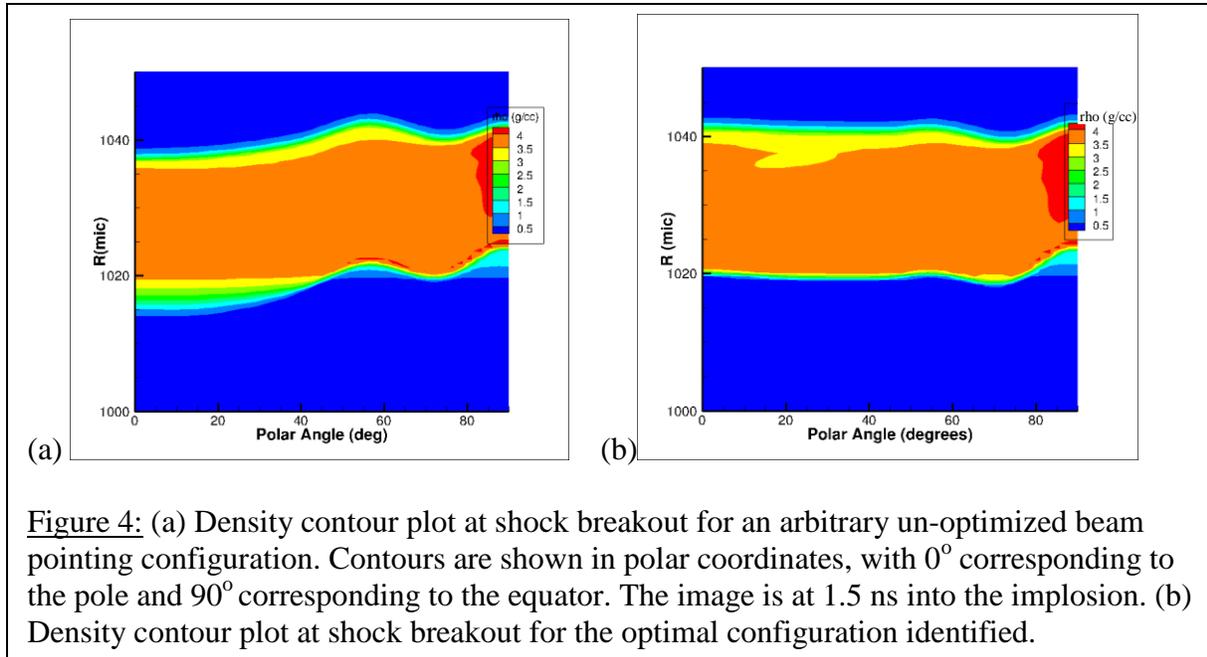
Figure 4: (a) Density contour plot at shock breakout for an arbitrary un-optimized beam pointing configuration. Contours are shown in polar coordinates, with 0° corresponding to the pole and 90° corresponding to the equator. The image is at 1.5 ns into the implosion. (b) Density contour plot at shock breakout for the optimal configuration identified.

In Figure 4b, the more uniform case, there is a small ripple near the equator. This occurs because the significant repointing of the laser beams results in reduced absorption at the equator and insufficient drive. This problem is difficult to fix solely with a re-pointing scheme. For example, as Ring 4 is repointed more toward the equator, more of its energy misses the target. A solution proposed to this problem is to engineer phase plates which would concentrate more energy locally at the equator [6]. These new phase plates will not be available for several years. However, the level of uniformity shown in Fig. 4b is adequate for the proposed preliminary experiments as the goal is to predictably model the symmetry of direct drive implosions on the NIF. The goal of achieving ignition will be pursued at a later stage. In Table 1, the final optimized beam pointing scheme, defocus length, and relative initial powers of the beams are shown. The distance Δr corresponds to the beam shift perpendicular to the beam axis and is given by $\Delta r = R_t \sin(\theta_r - \theta)$, where R_t is the target radius.

	Original Angle θ [deg]	Repointed Angle θ_r [deg] (Δr [mic])	Defocus Length	Energy Multiplier (Foot)
Ring 1	23.5	23.5 (0 mic)	1.0 cm	1.0
Ring 2	30.0	35.0 (96 mic)	1.0 cm	0.8
Ring 3a	44.5	46.0 (29 mic)	1.5 cm	0.8
Ring 3b	44.5	69.0 (275 mic)	1.0 cm	1.0
Ring 4	50.0	86.0 (647 mic)	1.0 cm	1.0

Table I: Parameters of the laser used to obtain the uniform shock breakout shown in Fig. 4b. The repointed angle gives the intersection of the beam axis with the initial target surface, and Δr gives the corresponding shift of the beam perpendicular to its axis

4. Beam Power Modifications

In order to control the shape of the imploding shell after shock breakout, the beam power must be modified. By changing the power in the polar and equatorial rings, control over the final shape of the shell can be established in simulations. Since the aim of the preliminary experiments on which these simulations were focused is simply to examine the feasibility of a controlled direct drive implosion for the NIF, it is necessary to demonstrate that some control over the final shape of the target can be established. Therefore, laser parameters have been identified in simulations that will produce three different shapes: prolate, where the poles lag behind the equator; spherical, which is round to within experimental error; and oblate, where the equator lags behind the poles. These shapes are shown in Figure 5(a,b,c).
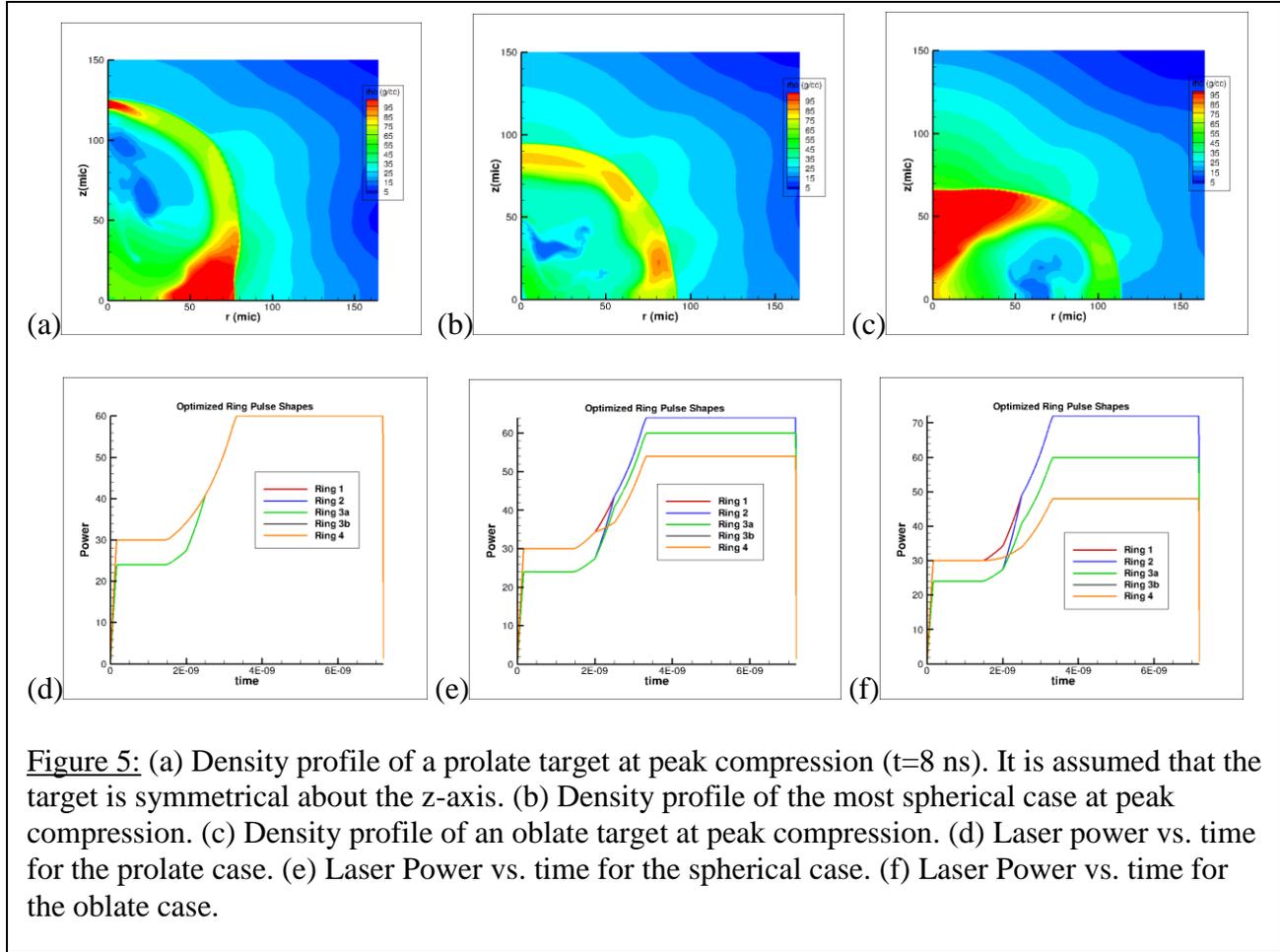
Figure 5: (a) Density profile of a prolate target at peak compression (t=8 ns). It is assumed that the target is symmetrical about the z-axis. (b) Density profile of the most spherical case at peak compression. (c) Density profile of an oblate target at peak compression. (d) Laser power vs. time for the prolate case. (e) Laser Power vs. time for the spherical case. (f) Laser Power vs. time for the oblate case.

Since the beam pointing configuration was already optimized to achieve a uniform shock at breakout, it is important to leave the foot unmodified. The laser power for each ring was modified only during the rise and main pulse to change the shape of the target after shock breakout. Figure 5(d, e, f) shows the pulse shapes of each ring for the prolate, spherical, and oblate cases. Notice that each of the three pulse shapes is identical during the foot. In order to achieve the three distinct final target shapes, the powers of the equatorial and polar rings were modified accordingly. For the prolate case, the power of each ring in the main pulse was left unmodified (Fig. 5b). For the oblate case, Rings 1 and 2 have higher power during the main pulse relative to Rings 3b and 4, while the power of Ring 3a was left unmodified. In order to

12

achieve a spherical shape, some fine-tuning of the ring powers was necessary, and the difference between the equatorial and polar rings is smaller (Fig. 5e).

The dynamics leading to the shape of the compressing core is a complicated combination of shock velocity and shell kinetic energy across different angular regions of the target. For instance, the initial configuration, which was then iteratively adjusted to provide the different shapes, resulted in a prolate shape for the compressed shell. As seen in Figure 4(b), the shock in the vicinity of the equator lags behind the rest of the target, meaning that it is traveling inwards at a lower velocity. Eventually this shock reaches the center of the target and begins to travel outwards again, and when it reaches the imploding shell, it causes the shell to impulsively decelerate. The shell soon stagnates and disassembles. However, the shock at the equator moves at a lower velocity than that at the poles, so it does not travel as far out after it has reached the center of the target before it meets the imploding shell. This means that the shell at the equator will implode farther than the shell at the poles before the target disassembles, creating the prolate shape seen in Figure 5a. This illustrates the importance of shock nonuniformity on the final shape of the compressed shell. The initial shock and shape of the target must be as uniform as possible in order to limit the additional complications introduced by the interaction of the nonuniform shock and the nonuniform converging shell.

5. Ablation Surface Position as an Experimental Measurable

The shape of the converging core can be obtained by using x-rays produced by an external source to image the high-density portion. [7] However, for these initial NIF experiments, x-rays emitted by the converging capsule will be used to study asymmetry. Simulations indicate that the maximum intensity in x-ray images for photon energies corresponding to ~2 keV corresponds closely to the ablation surface. [8] The ablation surface is important because it is

13

where the pressure that drives the shell inward is established by the laser. As mentioned earlier, when the laser beams irradiate the outer plastic shell of the target, they cause the target to heat up, and material from the outer shell begins to ablate. The rest of the target moves in like a rocket driven by the pressure set up by the ablating material. The ablation surface is defined as the location where this action occurs. As this location moves inwards during the implosion, the shell material spontaneously emits x-rays at a specific range of wavelengths, and by measuring the location where these x-rays are emitted, the location of the ablation surface can be determined. Thus, this provides an experimentally measurable quantity which provides useful information about the shape of the target.

While the x-ray self-emission images provide an observable, the quantity of direct-interest is the shape of the high-density shell. In these early experiments the high-density shell will not be directly imaged. It is, therefore, important to identify if the nonuniformity at the ablation surface is adequate to characterize the asymmetry. The difference between the locations of the ablation surface at the pole and the equator as a function of time is plotted in Fig. 6. This provides a measure of the nonuniformity of the ablation surface. The asymmetry of the high-density shell is characterized by the difference in the location of the center-of-mass of the shell between the pole and the equator. Fig. 6 also indicates that if the implosion were uniform and symmetric, this difference would be zero for all time. Both measures of asymmetry closely track each other till the end of the laser pulse (~7.2 ns), indicating that the ablation surface nonuniformity should provide equivalent information on shell asymmetry.
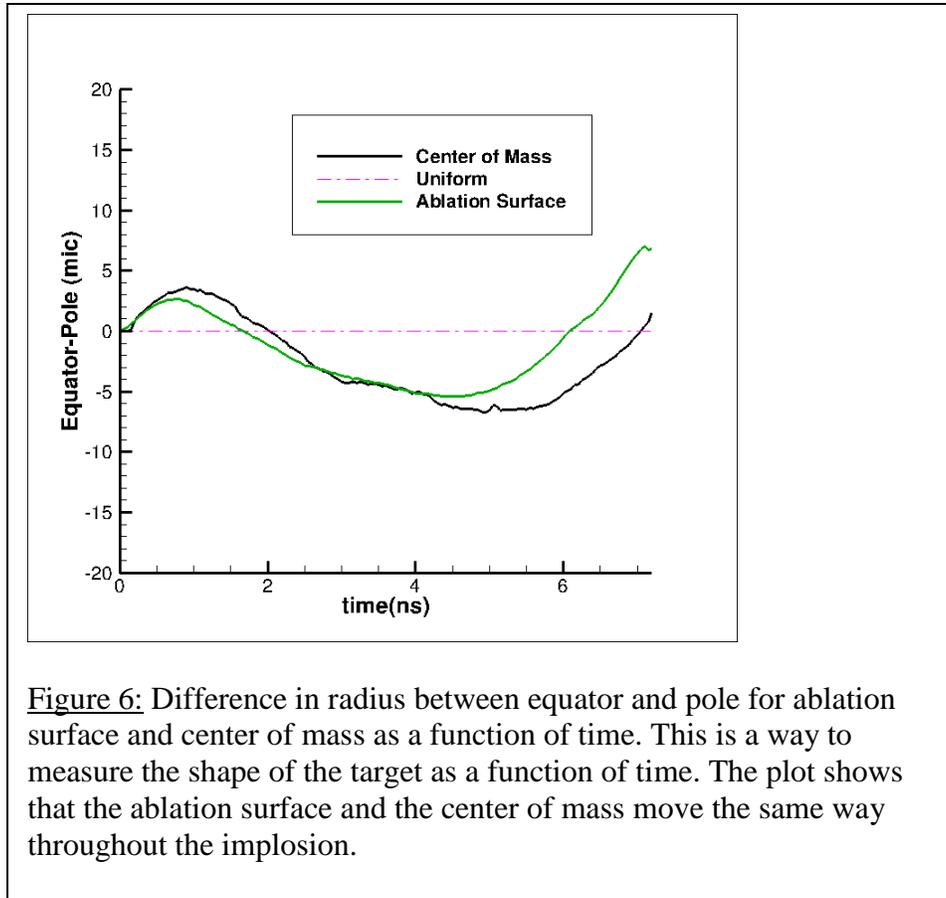
Figure 6: Difference in radius between equator and pole for ablation surface and center of mass as a function of time. This is a way to measure the shape of the target as a function of time. The plot shows that the ablation surface and the center of mass move the same way throughout the implosion.

The ablation surface position was determined for all three shapes achieved in simulations and plotted throughout time. Figure 7 shows the difference in ablation surface position plots for the prolate, spherical, and oblate cases as a function of time. It can be seen that the ablation surface differences follow what would be expected: for the prolate case (Fig. 7a), the pole lags behind the equator, and for the oblate case (Fig. 7c), the equator lags behind the pole, while for the spherical case (Fig. 7b), the difference remains less than 10 μm, corresponding to approximately 2.5% peak-to-valley in amplitude (the shell is approximately at 400 μm at the end of the laser pulse), which is smaller than the estimated error in the measurement. These graphs are only plotted to the end of the laser pulse at 7.2 ns because once the lasers stop irradiating the target, ablation no longer occurs and any measurement of the ablation surface would have no significance.

15

(a) (b) (c)
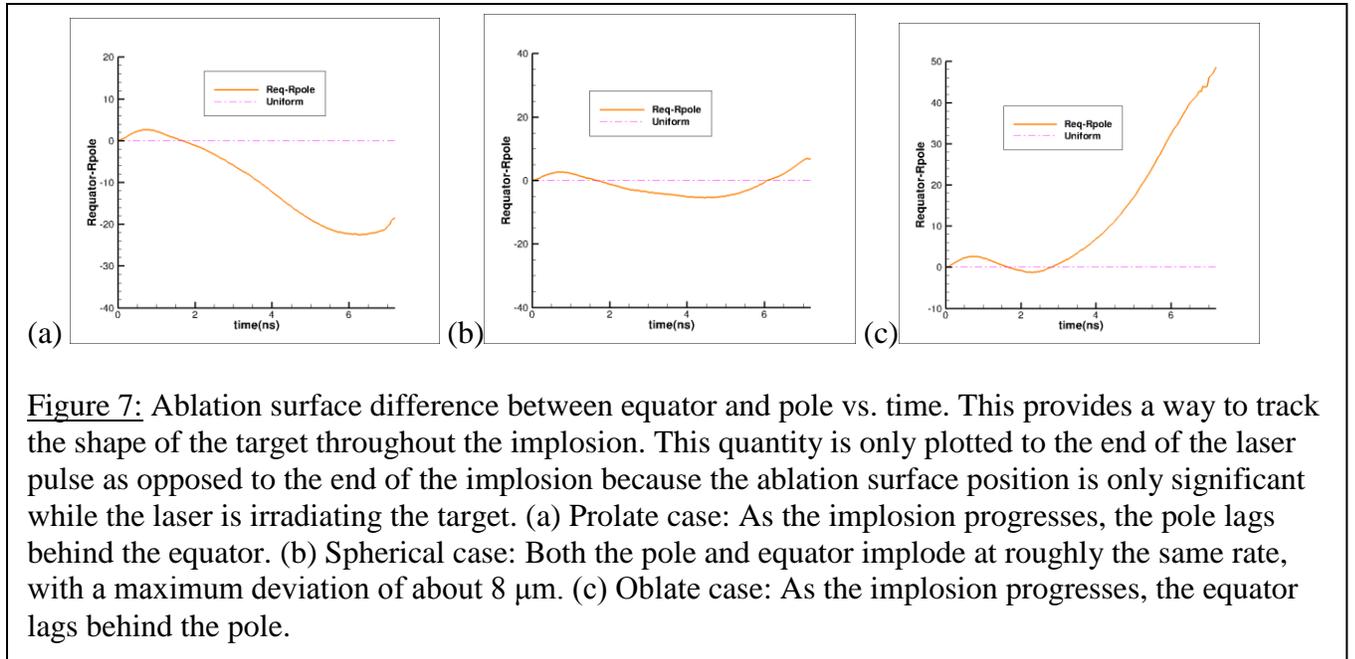
<u>Figure 7:</u> Ablation surface difference between equator and pole vs. time. This provides a way to track the shape of the target throughout the implosion. This quantity is only plotted to the end of the laser pulse as opposed to the end of the implosion because the ablation surface position is only significant while the laser is irradiating the target. (a) Prolate case: As the implosion progresses, the pole lags behind the equator. (b) Spherical case: Both the pole and equator implode at roughly the same rate, with a maximum deviation of about 8 μm. (c) Oblate case: As the implosion progresses, the equator lags behind the pole.

6. Sensitivity Tests

Uncertainties in the beam spot sizes can alter the dynamics of the implosion. Since Ring 4 beam profiles are the smallest of all the beam profiles and the most critical for irradiating the equator adequately, these beam sizes can have a significant impact on the shape.   Accurate measurements of the beam profiles have not yet been performed, and Ring 4 spot sizes could be larger in actuality than the ones used in these simulations. In order to examine the level of sensitivity of the target to spot size, simulations were conducted which used a Ring 4 beam profile which was 20% larger at best focus than the original, while keeping the same configuration used to achieve a spherical implosion. Figure 8 illustrates the results of this test, showing the density contour profile for the target at peak compression. It can be seen by comparing this figure with Fig. 5b that the compressed shell is now oblate instead of spherical.

16

Figure 8: Sensitivity test to 20% larger Ring 4 beam spot sizes. The original spherical pointing and pulse shapes were used, but Ring 4 spot sizes at best focus were made to be 20% larger. The density profile is shown at peak compression (8 ns). The target uniformity degrades considerably with the different spot size.
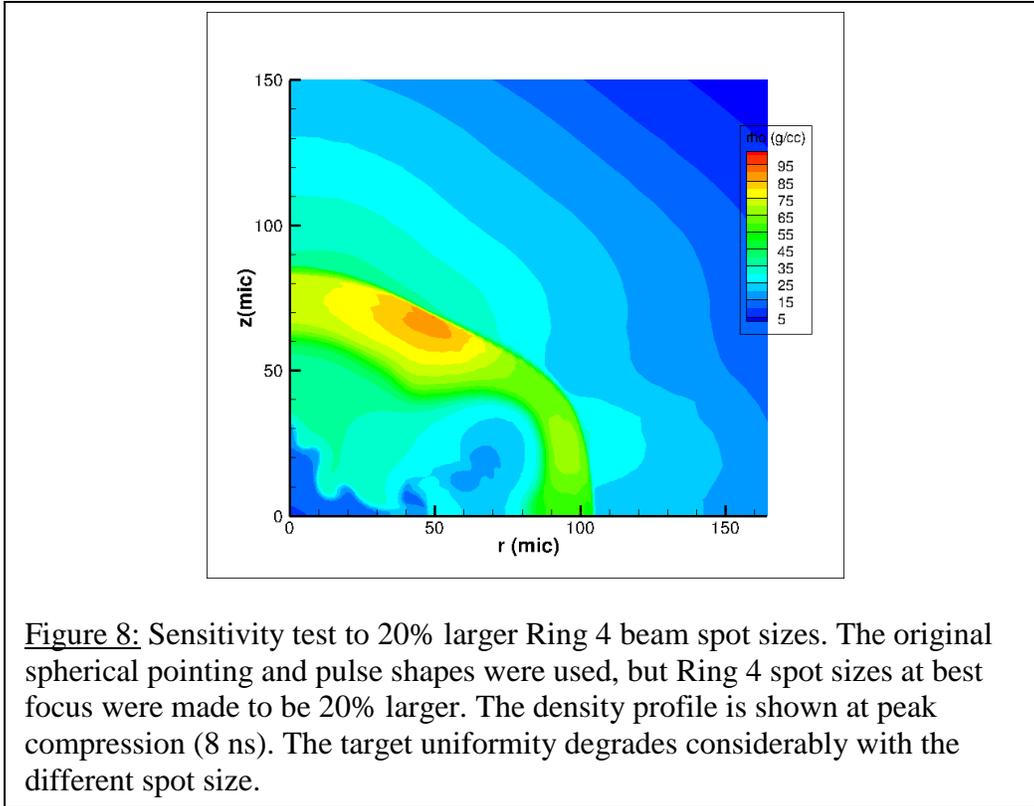
7. 50 μm-Shell Target Tests

Simulations were also performed using a similar target with a radius of 1100 μm, but a CH shell thickness of just 50 μm. The thinner shell causes it to implode much faster than the thicker 80 μm shell, which reduces the duration of the implosion. The higher implosion velocity is relevant for ignition target designs. This increased shell velocity also causes the shape of the target to be more difficult to control. However, despite this difficulty, a level of control over the final shape of the target was established by identifying the same three shapes as the original target: prolate, spherical, and oblate. The density profiles of these three cases at peak compression are shown in Fig. 9(a,b,c), respectively. An analysis of the beam pointings was done for the 50 μm shell target in the same fashion as was done for the 80 μm shell target, and it was found that the same beam pointing modifications produce an optimally uniform shock

17

breakout. Similar ring power changes were also used in both the 80 μm and 50 μm targets, although there are some subtle differences.
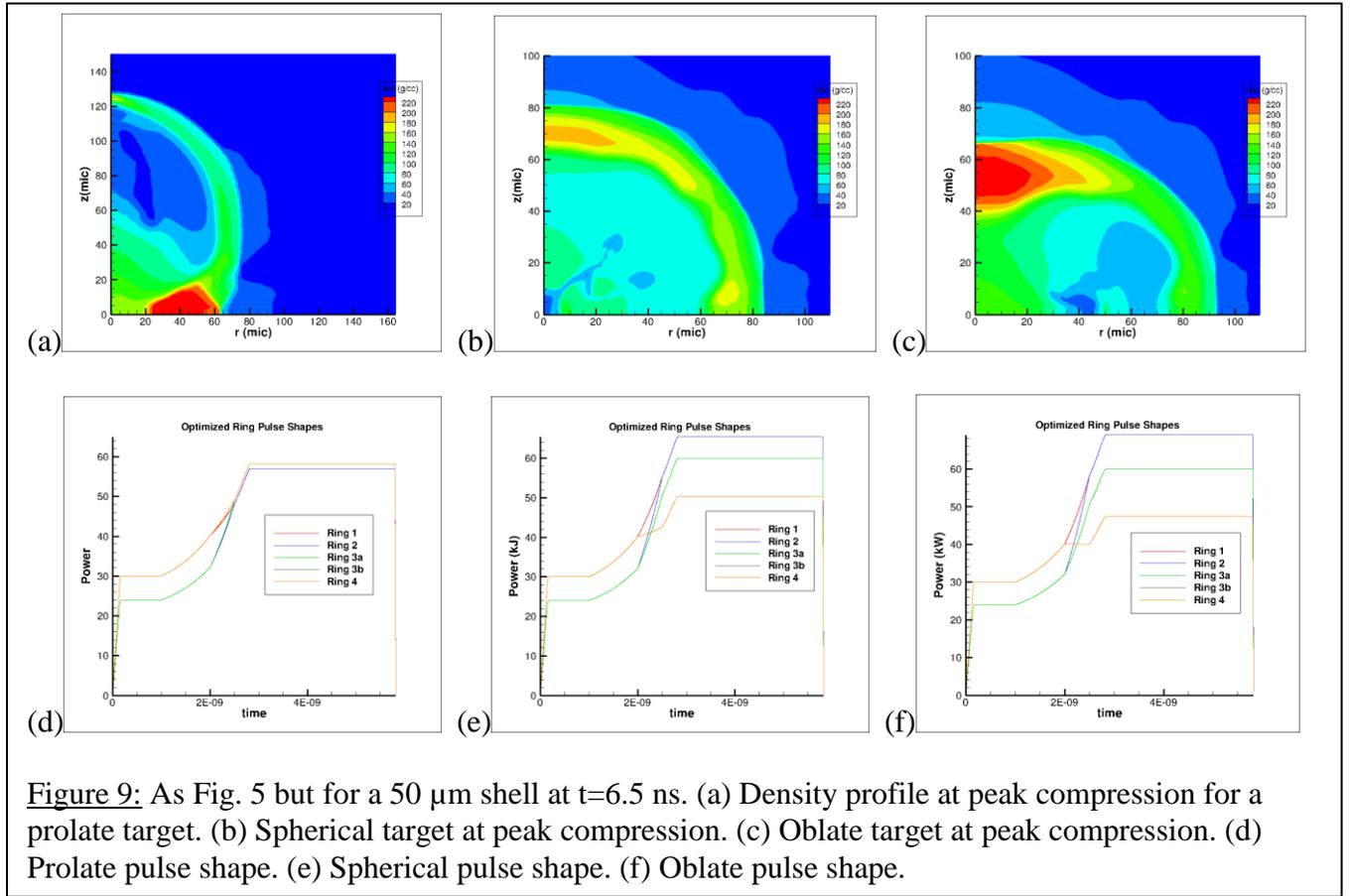
Figure 9: As Fig. 5 but for a 50 μm shell at t=6.5 ns. (a) Density profile at peak compression for a prolate target. (b) Spherical target at peak compression. (c) Oblate target at peak compression. (d) Prolate pulse shape. (e) Spherical pulse shape. (f) Oblate pulse shape.

An analysis of the location of the ablation surface was also performed for the 50 μm shell. The shape of the target was quantified in the same fashion as was previously done: the difference between the radii of the ablation surface at the pole and equator is calculated and plotted throughout time. Figure 10(a,b,c) shows these plots for the prolate, spherical, and oblate cases, respectively. It can immediately be seen that the shape of the shell varies much more in the 50 μm tests than in the 80 μm tests. In Fig. 10(b) it appears that the ablation surface is

actually demonstrating prolate characteristics. However, the density profile in Fig. 9(b) indicates that the parameters used produce a spherical shape at peak compression.

Figure 10: Ablation surface radius difference between equator and pole as a function of time for the 50-μm-shell target. (a) Prolate case. (b) Spherical case. (c) Oblate case.
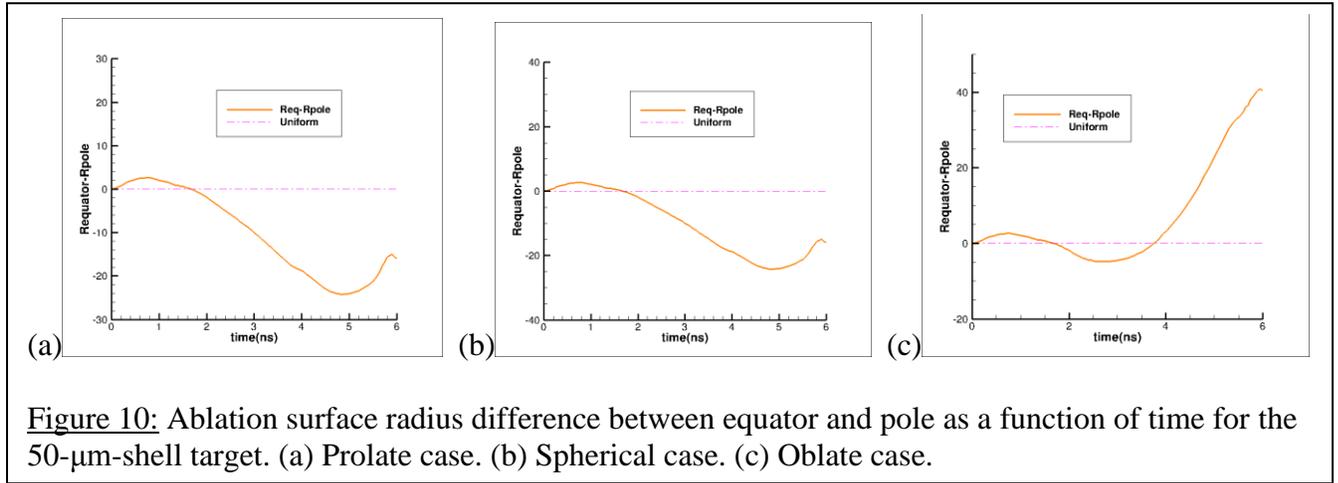
8. Conclusion

Experiments will be carried out on the National Ignition Facility to explore the direct drive method of inertial confinement fusion. In order to design these experiments and identify a configuration which yields an optimally uniform implosion, simulations were performed using *DRACO*, a 2-D hydrodynamics modeling code. These simulations investigated the pointing of the beams, the defocus length, and beam power modifications in order to obtain different shapes of the compressing shell. It was shown that the nonuniformity of the ablation surface position, an experimentally measurable quantity, is closely related to the overall shape of the target. Finally, the level of sensitivity of the shape of the shell to uncertainties in beam spot sizes was investigated and the resulting shape of the shell was found to be predictable.

9. Acknowledgements

I would like to thank those who helped me in the completion of my project and this paper. First, I would like to thank Dr. Stephen Craxton for giving me the opportunity to participate in this experience. His leadership and guidance during my time at the Laboratory for Laser Energetics were invaluable, and his suggestions helped me immensely to revise and refine this paper. Second, I would like to thank Dr. Tim Collins, who aided me while my advisor was away. Third, I would like to thank my fellow interns, who were eager to help when I had trouble with my work and who made my experience enjoyable and fulfilling. I would also like to thank my parents for encouraging me to pursue this experience and for being supportive both through the application process and during the internship. Finally, I would like to give a special thanks to my advisor, Dr. Radha P. Bahukutumbi, both for her role in designing and focusing my project and for spending countless hours working to help me understand and overcome difficulties I faced with my work. Her research is advanced and time-consuming, yet she chose to spend time mentoring me so that I could make my own contribution, and for that I am extremely grateful.

References:

1.J. Nuckolls, L. Wood, A. Thiessen, and G. Zimmerman, Nature **239**, 139 (1972).

2. T. R. Boehly et al., J. Appl. Phys. **85**, 3444 (1999).

3. E. Moses, "The NIF: An International High Energy Density Science and Inertial Fusion User Facility", presented at The Seventh International Conference on Inertial Fusion Sciences and Applications, Bourdeaux-Lac, France 12-16 September 2011.

4. A. M. Cok, R. S. Craxton, and P. W. McKenty, Phys. Plasmas **15**, 082705 (2008).

5. P. B. Radha et al., Phys. Plasmas **12**, 032702 (2005).

6. J. A. Marozas et al., Phys. Plasmas **13**, 056311 (2006).

7. F. J. Marshall et al., Phys. Rev. Lett. **102**, 185004 (2009).

8. D. T. Michel et al., Rev. Sci. Instrum. **83**, 10E530 (2012).